



The structure and fluorescence properties of polypropylene/carbon quantum dot composite fibers

Banafsheh Safaie¹ · Mostafa Youssefi¹ · Behzad Rezaei²

Received: 7 October 2020 / Revised: 31 December 2020 / Accepted: 27 January 2021 /
Published online: 4 February 2021

© The Author(s), under exclusive licence to Springer-Verlag GmbH, DE part of Springer Nature 2021

Abstract

Carbon quantum dot (CQD)/polypropylene (PP) nanocomposite fibers were fabricated using the melt spinning technique. The composite fibers were studied using tensile measurements, wide-angle X-ray diffraction patterns, Fourier transform infrared spectroscopy, fluorescence spectrophotometry, scanning electron microscopy, transmission electron microscopy, and reflection spectrophotometry. The effects of CQDs size, CQD/matrix interface adhesion, and CQD loading on the structure, mechanical, orientation, and optical properties of PP/CQD nanocomposite fibers were investigated using Taguchi experimental design. The produced PP/CQD nanocomposites fibers exhibited color emission under excitation energy, which could be attributed to the presence of CQDs embedded inside the PP matrix. The photoluminescence emission spectra of the nanocomposite fibers containing smaller-size CQD nanoparticles were more significant than other samples at the wavelength of 347 nm. The results of reflection spectrophotometry measurements showed that the purity value was increased with enhancing CQD loading inside the polymer matrix. The results also demonstrated a yellowish red hue imparted to the nanocomposite fibers with improving CQD loading inside the polymer matrix. The amount of redness and yellowness of PP/CQD nanocomposite fibers was lower for the smaller-size nanoparticles and tended to blue and green color. The produced fibers could be easily fabricated and used potentially in a variety of applications like photochemical reactions, anti-counterfeiting, optoelectronic devices, etc.

Keywords Polypropylene · Carbon quantum dot · Fluorescence · Composite fibers

✉ Mostafa Youssefi
youssefi@cc.iut.ac.ir

¹ Department of Textile Engineering, Isfahan University of Technology, 84156-83111 Isfahan, Iran

² Department of Chemistry, Isfahan University of Technology, 84156-83111 Isfahan, Iran

Introduction

Nanocrystalline materials of physical dimensions smaller than the exciton Bohr radius are called quantum dots (QDs). The size of QDs in the nanometer region affects the electronic properties of them [1]. They have the potential for a variety of applications such as fluorescent labeling for medical diagnosis, bio-imaging, energy and optical sensing, and optical amplification due to their specific optical and electrical properties [2–6]. On the other hand, a new member of the carbon family is carbon quantum dots (CQDs). CQDs have chemical stability, compatibility, low toxicity, aqueous solubility, optical absorptivity, and easy functionalization [7–10].

Because of the specific optical and electrical properties of CQDs, they can be used as nanofillers in polymer composites. Preparation of polymer/CQD nanocomposites and determination of their physical properties have been the subject of many studies [11–13]. Polymer/CQD nanocomposites are used in a variety of applications such as high-performance aircraft and sensors, smart clothing, and tagging [14–16]. Besides, they can be used as fluorescent textile fibers. There are several investigations on the preparation of polymer/QDs composite nanofibers and the determination of their physical properties [17–19]. By the way, the main challenge is the dispersion of QDs in the polymer matrix and achieving the favorite optical properties in composite fibers.

There are few studies regarding the synthesis and properties of PP/CQD nanocomposite fibers. Thus, the present research work's main objective was to determine the properties of PP fibers containing CQDs nanofiller as a fluorescent labeling substance. Also, the effects of essential parameters (CQD percentage, CQD size, and compatibilizer percentage) on the properties of PP/CQD fiber were evaluated. An experimental design technique was used to examine the effects of the mentioned parameters on the structure and properties of the nanocomposite fibers. The Taguchi method was used for the experimental design. The obtained results from the experimental design could lead to achieving process optimization.

Experimental

Materials

PP with the melt flow index (MFI) of 25 g/10 min (230 °C and 2.16 kg) was purchased from Marun Petrochemical Company, Iran. The maleic anhydride grafted PP (PP-mg) with 30% maleic anhydride was prepared from Marun Petrochemical Company, Iran, and was used as a compatibilizer. Chitosan ($C_6H_{11}NO_4$)_n, with MW of 100,000–300,000 g/mol, was purchased from Acros, and acetic acid 99.9% was received from Merck.

Synthesis and characterization of carbon QDs

CQDs were synthesized from chitosan following the procedure reported elsewhere (Fig. 1) [19]. Chitosan was dissolved in acetic acid and heated at 180 °C in

a Teflon-coated stainless steel autoclave for 8 and 16 h. After cooling to room temperature, the obtained dark brown product was centrifuged for 25 min at 14,000 rpm to remove the higher size particles with less fluoresce property. The average size of the CQDs used in this study was 5 nm (production time: 16 h) and 2 nm (production time: 8 h).

Experimental design

The purpose of experimental design is to observe and identify output changes by consciously changes input variables. There are several ways to experimental design. Taguchi experimental design is the method to improve the quality of the process and achieve the product. Taguchi experimental design is organized based on the minimum resources, time, and the number of possible experiments. The steps of Taguchi experimental design implementation, considering the details, and in order of importance, are as follows: introducing effective factors in the reaction, the number of required experimental, analysis of answers. Taguchi’s L8 array method was used for the design of the experiments. Three factors were considered for the evaluation of the response variables: one factor in 4 levels (CQD nominal weight percentage 0%, 0.5%, 1%, and 2%) and two factors in 2 levels (CQD size 2 nm and 5 nm and compatibilizer percentage 0% and 3%). Taguchi’s L8 array is defined in Table 1. The Taguchi experiment proposed arrays of 8 rows and three columns for three factors (factor 1: percentage of the CQDs, factor 2: CQDs size, and factor 3: percentage of the compatibilizer) [20].

Preparation of PP/CQD nanocomposites

The PP/CQD nanocomposites were prepared by melt mixing in a twin-screw extruder (ZSK twin-screw extruder, with $L/D=40$). Rotation speed was 120 rpm, and the temperature of 6 thermal zones was 195, 200, 210, 210, 200 °C, respectively. According to the Taguchi experimental design, eight samples were prepared with varying amounts of CQDs (0.5%, 1%, and 2% w/w), two different CQDs sizes, and two concentrations of compatibilizer (0% and 3% w/w). Fiber spinning was carried out by a Fourne-Bonn melt spinning machine. The temperature of five thermal zones was set at 215, 220, 225, 230, 235 °C, respectively.



Fig. 1 Schematic for the synthesis of carbon quantum dots from chitosan

Table 1 Taguchi array for the design of the experiments

<i>n</i>	% CQD	CQD size	% Compatibilizer (PP-mg)
1	1 level=0%	1 level=5 nm	1 level=0%
2	1 level=0%	2 level=2 nm	2 level=3%
3	2 level=0.5%	1 level=5 nm	1 level=0%
4	2 level=0.5%	2 level=2 nm	2 level=3%
5	3 level=1%	1 level=5 nm	2 level=3%
6	3 level=1%	2 level=2 nm	1 level=0%
7	4 level=2%	1 level=5 nm	2 level=3%
8	4 level=2%	2 level=2 nm	1 level=0%

Characterization

The tensile properties of the fibers were measured by a Zwick (1446-Germany) tensile tester. The gauge length and test speeds were 2.54 cm and 60 mm/min, respectively. A Bomem MB100 FTIR spectrometer was used to record the FTIR spectra between 4000 and 400 cm^{-1} in transmission mode. The resolution of the spectrometer was 4 cm^{-1} , averaging 32 scans. Wide-angle X-ray diffraction patterns of the samples were obtained using a Philips X-ray diffractometer model Xpert MPD with symmetrical reflection geometry ($\text{CuK}\alpha$ radiation, $\lambda=1.5418\text{\AA}$, voltage 40 kV, current 30 mA). Birefringence of the fibers was measured using a Zeiss polarizing microscope equipped with a 30th-order tilting compensator. Photoluminescence emission of the samples was measured using a LS50B Luminescence Spectrometer (Edinburgh Instruments, UK). The reflection curve of the samples was obtained using a Texflash spectrophotometer from the Datacolor Company, USA. The fibers were prepared in parallel and placed in the spectrophotometer. Due to the samples' transparency, the reflection measurements were performed on both white and green background standards of the spectrophotometer device with the D65 source of ultraviolet light. The nanocomposite fibers' morphology was studied by a field emission scanning electron microscope (FESEM: Hitachi S-4160, Japan) and a transmission electron microscope (TEM: JEM 3010, JEOL, Japan). For SEM images, the fibers were coated with gold using the sputtering technique. The ultra-microtomy method was used for cutting the specimens for TEM. Fluorescence microscopic images were obtained using a fluorescence microscope (Eclipse Ti-U, Nikon, Japan).

Results and discussion

Morphology of the nanocomposite fibers

Figure 2 shows the FESEM images of the samples n3, n5, and n7. It can be seen that the CQDs were embedded inside the PP matrix, indicating the CQDs had an

excellent wetting with the PP matrix. Figure 3 presents the TEM images of the nanoparticles inside the PP matrix. Since the CQDs were less transparent toward the electron beam compared to the polymeric materials, the CQDs appeared black or dark gray. CQDs were surrounded by the polymer in gray color. The CQDs diameter was about 2.9 and 6.1 nm for n4 and n5 samples, respectively.

FTIR spectra

Figure 4 shows the FTIR spectra of the samples. The absorption peaks in the range of 2800–3100, 1380, and 1460 cm^{-1} are related to CH, CH_3 , and CH_2 . In the maleic anhydride grafted PP (PP-mg), the absorption peaks in the region of 1600–1800 cm^{-1} are related to the carbonyl group in the ring of anhydride, adsorption in the region of 2600–2700 cm^{-1} , and strong adsorption in the range of 1000–1300 cm^{-1} are related to C–H bond and C–O bond in maleic anhydride ring, respectively [21–23]. In the samples containing carbon quantum dots, the adsorption peak of about 3400 cm^{-1} is related to the O–H vibration bond, indicating the existence of C–OH in the carbon quantum dots. The adsorption peak that appeared at 3390 and 1790 cm^{-1} can be assigned to symmetrical stretching and vibrational deformation of $-\text{NH}_2$ on carbon quantum dots' surface. The sharp peak at 1430 and 1630 cm^{-1} confirmed the formation of C=O and C–N groups in

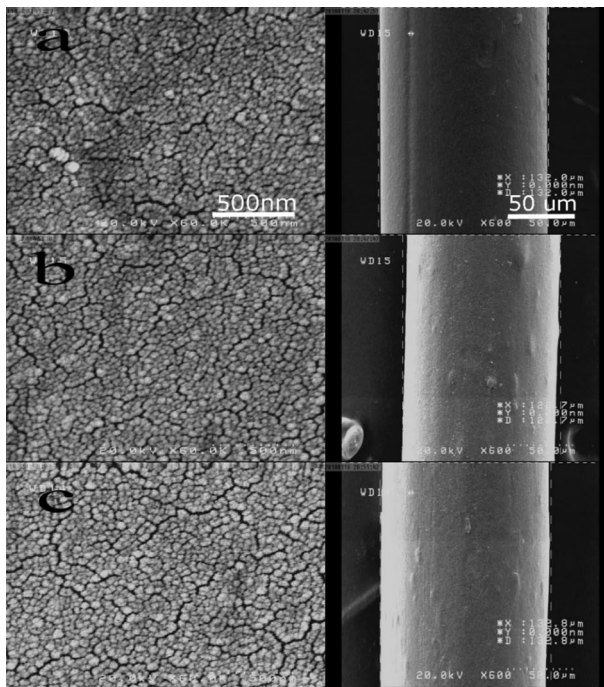


Fig. 2 The scanning electron micrographs of the surface of the nanocomposites (**a** n3, **b** n5, **c** n7)

Fig. 3 The transmission electron micrographs of the nanocomposites fiber (a n4, b n5)

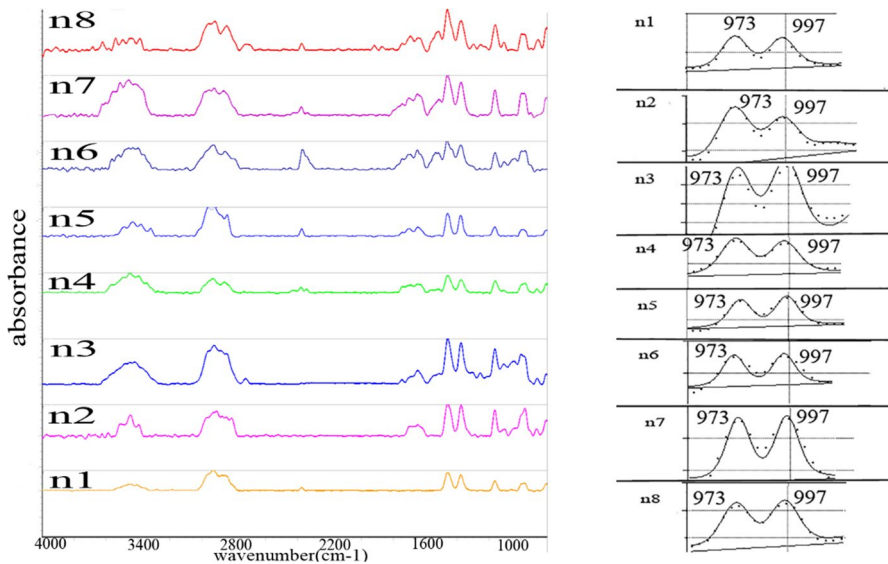
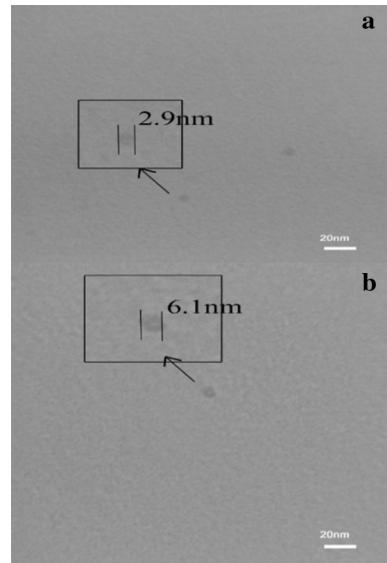


Fig. 4 FTIR spectra of the nanocomposite fibers

the PP/CQD nanocomposite fibers [19, 24]. Schematic for the chemical reaction in the synthesis of PP/CQD nanocomposites is shown in Fig. 5. In our previous work, the interphase properties of polypropylene/carbon quantum dot nanocomposite fibers are investigated using micromechanical modeling [20].

The peaks at 973 cm^{-1} and 997 cm^{-1} correspond to the amorphous phase and the alpha-crystalline phase, respectively [25]. The absorbance ratio A_{997}/A_{973} was used to determine the samples' helical content [25]. The PP/CQD nanocomposite fibers' helical content obtained from the absorbance ratio A_{997}/A_{973} is summarized in Table 2.

Figure 6 shows the Taguchi design analysis for the helical content of the samples. As can be seen, the helical content of the samples was increased with an increase in CQD content. The sample containing the smaller-size nanoparticles showed a higher helical content of nanocomposite fibers. The sample containing the compatibilizer exhibited lower helical content. The obtained results for the helical content of the samples were in accordance with the degree of crystallinity of them obtained from WAXD data. Therefore, it could be stated that in melt spinning PP/CQD nanocomposite fibers, CQDs caused a significant impact on the composite fiber structure and morphology [26].

Birefringence

The results of the Taguchi design analysis of the birefringence data for the composite fibers are shown in Fig. 7. The birefringence of the nanocomposite fibers was higher than that of the neat PP. Besides, the birefringence of the nanocomposite fibers was increased with the increase in their CQD content. The nanocomposite fibers containing the smaller-size CQDs showed a higher birefringence value. Furthermore, the addition of the compatibilizer increased the birefringence of nanocomposite fibers. The obtained results were in accordance with the results obtained

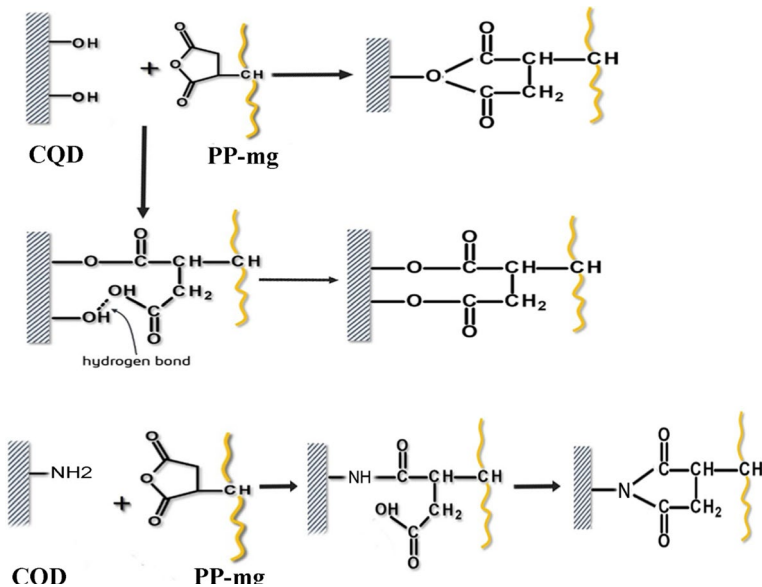


Fig. 5 Schematic of the chemical reactions for the synthesis of PP/CQD nanocomposites

Table 2 The experimental results for PP/CQD samples

<i>n</i>	E-modulus (MPa) [CV%]	Tensile strength (MPa) [CV%]	Strain (%) [CV%]	Linear density (Tex) [CV%]	Birefringence [CV%]	Crystallinity (%) [CV%]	Helical content [CV%]
1	931.92 [20.21]	27.10 [18.82]	785.7 [23.64]	19.10 [3.1]	0.0049 [6.00]	0.54 [7.86]	0.70 [7.15]
2	994.89 [19.70]	26.25 [14.88]	828.8 [14.33]	19.39 [2.6]	0.0067 [1.91]	0.34 [22.98]	0.63 [7.93]
3	950.71 [22.68]	24.61 [14.03]	967.6 [18.47]	22.57 [5.7]	0.0062 [2.76]	0.48 [9.54]	0.90 [6.66]
4	1449.31 [11.69]	41.10 [12.44]	1164.6 [13.12]	18.39 [8.9]	0.0056 [3.85]	0.62 [7.52]	1.05 [4.76]
5	1613.29 [30.74]	40.33 [16.04]	940.9 [10.28]	14.63 [7.5]	0.0081 [8.76]	0.43 [14.38]	0.91 [5.49]
6	1121.2 [14.70]	27.53 [12.12]	888.4 [11.10]	19.73 [5.0]	0.0076 [19.82]	0.61 [5.69]	0.99 [5.05]
7	1057.48 [14.90]	24.87 [20.31]	670.8 [25.98]	15.73 [9.9]	0.0061 [2.99]	0.42 [22.44]	0.90 [5.55]
8	1163.56 [21.35]	31.13 [17.42]	808.3 [18.15]	16.53 [18.4]	0.0059 [18.12]	0.55 [7.35]	0.99 [6.06]

^aCoefficient of variation

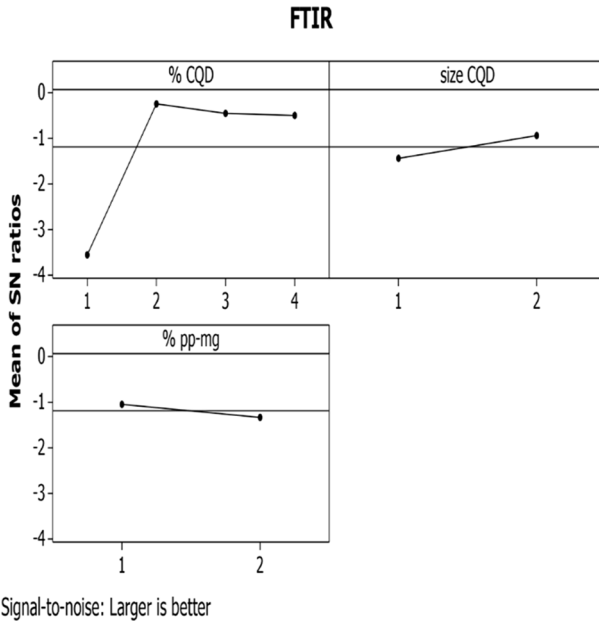


Fig. 6 Taguchi design analysis of the helical content from FTIR measurements

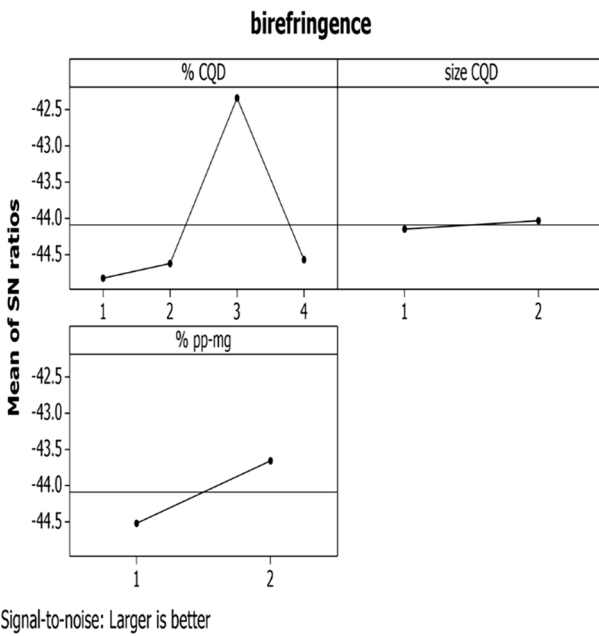


Fig. 7 Taguchi design analysis of birefringence data of the nanocomposite fibers

from the tensile measurements. The birefringence data of the PP/CQD nanocomposite fibers are summarized in Table 2.

Wide-angle X-ray diffraction

Figure 8 shows the wide-angle X-ray diffractograms of the nanocomposite fibers in 8 levels of Taguchi design. The composite fibers displayed characteristic diffracting peaks at $2\theta = 13.9^\circ$, 16.7° , 18.3° , and 21.6° corresponding to the planes (1 1 0), (0 4 0), (1 3 0), and (1 1 1) of its α -phase crystallite [27]. In other words, no change in the crystalline structure of the polymer due to the addition of CQDs into the polymer matrix was observed. The degree of crystallinity (X_c) was determined using the Hermans and Weidinger equation [27]:

$$X_c = \frac{1}{\left(1 + 1.207 \frac{Q_{am}}{Q_{cr}}\right)} \quad (1)$$

where Q_{cr} and Q_{am} are the area under crystalline and amorphous peaks, respectively.

Figure 9 shows the Taguchi design analysis for the degree of crystallinity of the samples. As can be seen, the sample containing 0.5% wt. CQDs, the CQDs size of 2 nm, and without compatibilizer exhibited the highest degree of crystallinity. It seemed that the CQDs had a nucleating effect inside the polymer matrix, and the crystallites were formed around the nanoparticles [28, 29]. As a consequence, the total crystallinity of the nanocomposite samples was higher than that of the sample

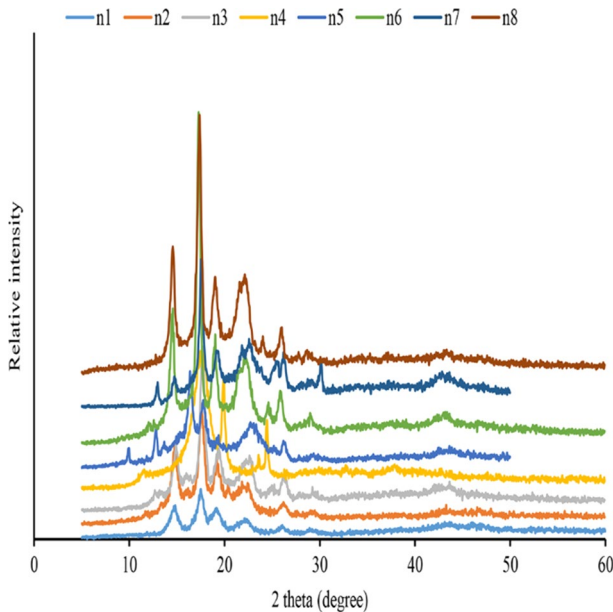


Fig. 8 Wide-angle X-ray diffractograms of the nanocomposite fibers

without carbon quantum dots (control sample). The degree of crystallinity of the samples was decreased by increasing the concentration of CQDs. The accumulation of nanoparticles was increased by increasing the amount of carbon quantum dots in the matrix due to the high interaction between the nanoparticles. The nucleating sites were reduced in the matrix with the accumulation of nanoparticles, and consequently, the percentage of crystallization in the nanocomposite is diminished. The sample containing the smaller-size nanoparticles exhibited a higher degree of crystallinity, which could be attributed to the presence of more nanoparticles acting as nucleating sites [20]. Also, the sample containing compatibilizer showed a lower degree of crystallinity, which might be due to the maleic anhydride groups in the compatibilizer structure. The degree of crystallinity of the PP/CQD nanocomposite fibers obtained from the wide-angle X-ray diffractograms is summarized in Table 2.

Tensile properties

Young’s modulus and tensile strength of the PP/CQD nanocomposite fibers obtained from the tensile experiments are summarized in Table 2. Taguchi design analysis was performed to obtain the dependent variables of the specified factors (CQDs percentage, CQDs size, and compatibilizer percentage). It was found that the sample with 1% wt. CQD, the CQD size of 2 nm, and 3% wt. compatibilizer exhibited the highest tensile strength (Fig. 10). Besides, as illustrated in Fig. 11, Young’s modulus of all of the nanocomposite fibers was higher than that of the neat PP fiber.

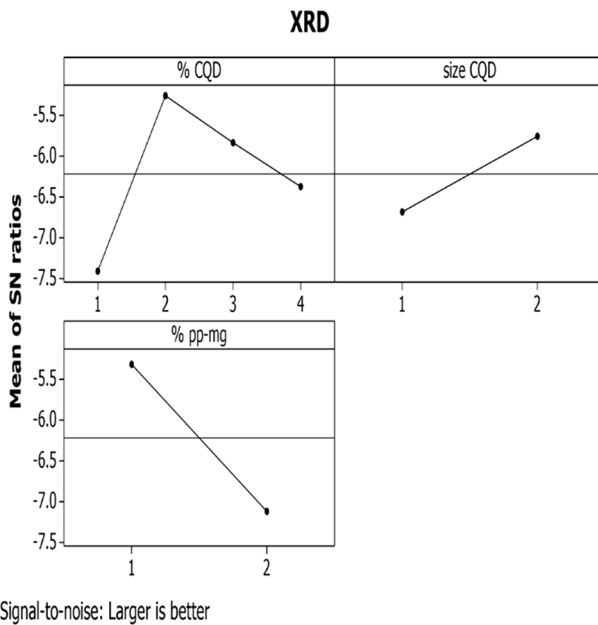


Fig. 9 Taguchi design analysis of crystallinity from XRD measurements

Therefore, it could be concluded that the addition of CQDs to the polymer matrix led to an increase in Young's modulus of the composite fibers. The highest modulus was achieved for the sample containing 1% wt. CQD, 2 nm CQD size, and 3% wt. compatibilizer. The increase in the tensile strength of the nanocomposite fibers could be due to the nanoscale dimensions of CQDs (high surface-to-volume ratio) as well as the enhancement of the interface of PP-CQD, which led to a better stress distribution [30–32]. CQDs aggregation in the sample containing 2% wt. CQD resulted in the reduction of its breaking stress and Young's modulus. This reduction could be attributed to the formation of stress concentration points [33–35]. The nanocomposite fibers containing smaller-size CQD nanoparticles exhibited higher tensile strength and modulus than the others. This indicated the critical effect of nanoparticle size on the tensile properties of composite fibers. Moreover, the samples containing compatibilizer showed higher tensile strength and modulus values. Therefore, it could be said that the addition of the compatibilizer improved the nanoparticles dispersion in the polymer matrix [20].

Fluorescence spectrometry

According to the reported data, the as-prepared CQDs possess excitation-dependent PL emissions [19]. Thus CQDs-polymer nanocomposite fibers are also expected to exhibit the same characteristic PL performance. The Taguchi design analysis for the PL emission spectra of PP/CQD nanocomposites is demonstrated in Fig. 12. The

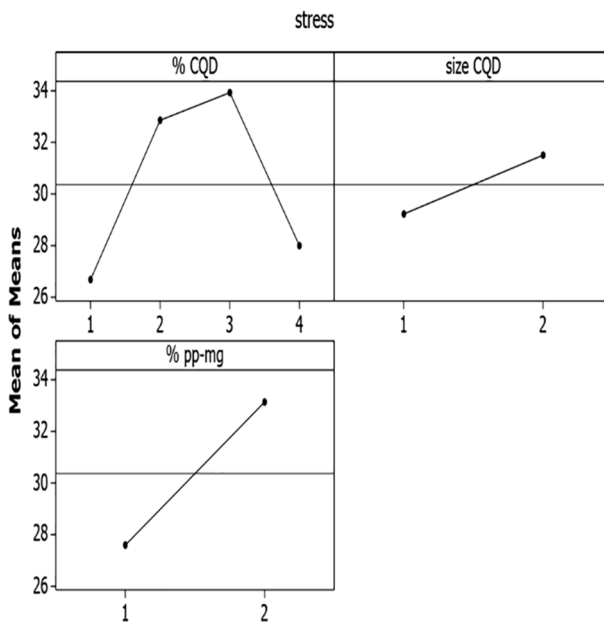


Fig. 10 Taguchi design analysis for the tensile strength of the nanocomposite fibers

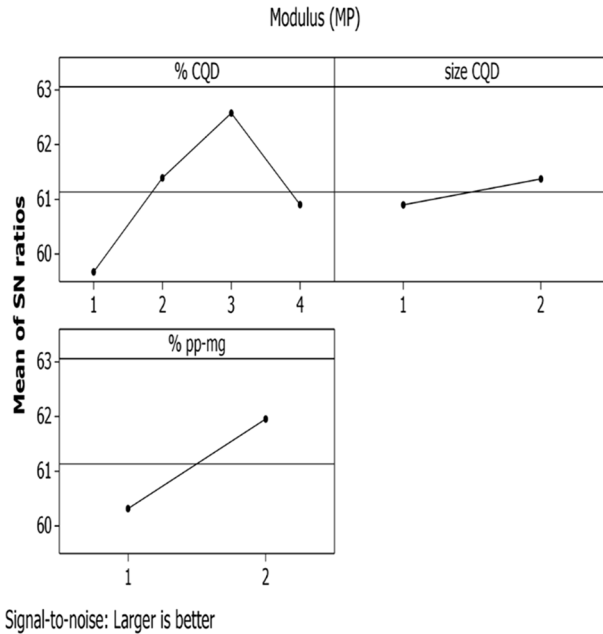
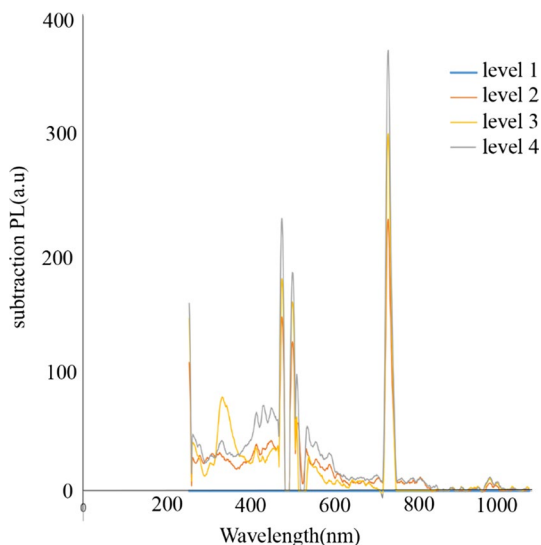


Fig. 11 Taguchi design analysis for Young’s modulus of the nanocomposite fibers

PP/CQD nanocomposites were excited at the wavelength of 250 nm. The fluorescence property of CQDs is susceptible to their concentration. The intensity of the emitted light increased with the increase in CQD content in the polymer matrix at the wavelength of 487 nm, 513 nm, and 745 nm. With increasing the CQD concentration from 1 to 2 wt.%, the emission peak of the PP/CQD nanocomposites shifted from 347 to 445 nm. The PL peak position showed small variation due to the incorporation of CQDs. A redshift in PL peak was expected if the CQDs were aggregated within the polymer matrix [36]. The PL behavior of the CQDs was excitation dependent, and the maximum absorption of CQDs is related to the size of CQDs, aggregation of CQDs in the polymer matrix, and the interaction between CQDs and the polymer matrix [37, 38]. The PL emission property is due to the size of the CQDs, the availability of sp^2 sites, the aromatic conjugated structure, and the structure’s defects. Besides, the presence of different sizes and multiple surface emissive trap status may cause inter-system crossing and adjacent vibrational relaxation of excited electrons, thus activating PL emission with the corresponding energy. So, a polymer blended with CQDs is also expected to show the same characteristic PL performance [39].

Figure 13 shows the effect of the compatibilizer’s addition on the PL emission spectra of the samples. The addition of the compatibilizer could affect the PL emission spectra of the nanocomposites. The compatibilizer could increase the PL emission spectra with the dispersion of CQD within the polymer matrix. According to the references [40, 41], the compatibilizer’s addition could increase interactions between the polymer chains and the nanoparticles. The resonance energy transfer

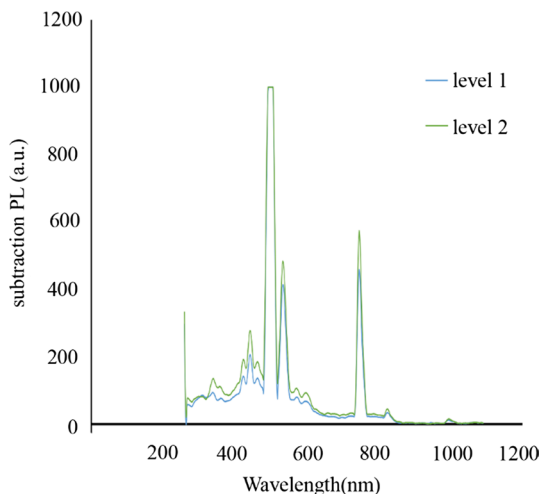
Fig. 12 Taguchi design analysis of emission spectra of PP/CQD nanocomposite excited at the wavelength of 250 nm as a function of the concentration of the CQDs



between neighboring nanoparticles decreases with the dispersion of CQDs inside the polymer matrix, so the light emitted from the surface of the nanocomposite increases.

The PL emission spectra did not significantly differ for the samples with different nanoparticle sizes (Fig. 14). The PL emission spectrum of the level 2 sample was greater than that of the level 1 sample at the wavelength of 347 nm. At longer wavelengths (red region), the PL peaks' intensity was lower for the smaller-size nanoparticles than the larger CQDs. In other words, the PL emission spectra were depended on the size of CQDs. As mentioned before, the optical properties of CQD depend on their size in the nanometer region.

Fig. 13 Taguchi design analysis of emission spectra of PP/CQD nanocomposite excited at the wavelength of 250 nm as a function of the concentration of compatibilizer

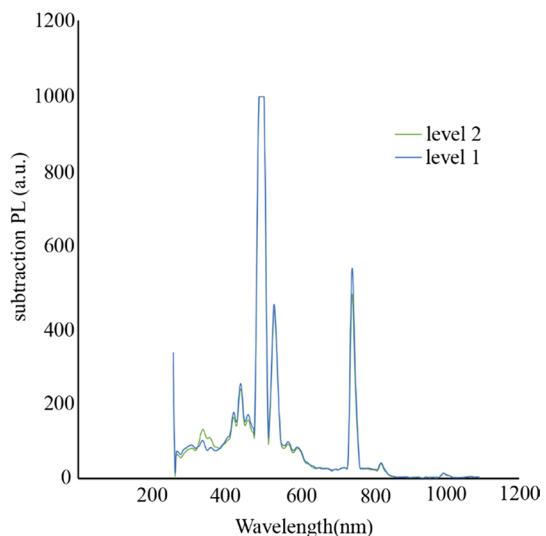


Fluorescence microscopic images were also captured by exciting the samples with three different filters at approximately 300, 455, and 530 nm, as shown in Fig. 15. The color emissions from the composite fibers confirmed the uniform distribution of CQDs in the polymer matrix. The photoluminescence behavior of CQDs was well detected inside the PP/CQD nanocomposite fibers. Therefore, the uniformity of the color emissions throughout the PP/CQD nanocomposite fibers implied the uniform distribution of CQDs without aggregation in the polymer matrix. In addition, the characteristic photoluminescence behavior of CQDs was well preserved inside the PP fiber matrix.

Reflection spectrophotometry

The light reflection of PP/CQD nanocomposite fibers was measured on the CIELAB color space [42, 43]. The Taguchi design analysis of color purity value (C^*) of the samples is shown in Fig. 16. It was observed that the purity value was increased with enhancing CQD loading inside the polymer matrix. This increase was apparent for the nanocomposite samples placed on both of the background standards. The increase in the purity value of the samples could be attributed to the color shade of CQDs inside the polymer matrix. In other words, the photoluminescence and color property of the CQDs were not eliminated when they were surrounded by the polymer matrix chains. The compatibilizer's addition increased the purity value of nanocomposite fibers due to the improved dispersion of the CQDs inside the polymer matrix. The sample containing the smaller-size nanoparticles showed a slightly lower purity value. It was implied that the effect of nanoparticle size on the color purity of the nanocomposite fibers was not significant. The results showed that CQDs' optical properties were preserved inside the nanocomposite fibers [8, 44].

Fig. 14 Taguchi design analysis of the emission spectra of PP/CQD nanocomposite excited at the wavelength of 250 nm as a function of CQDs size



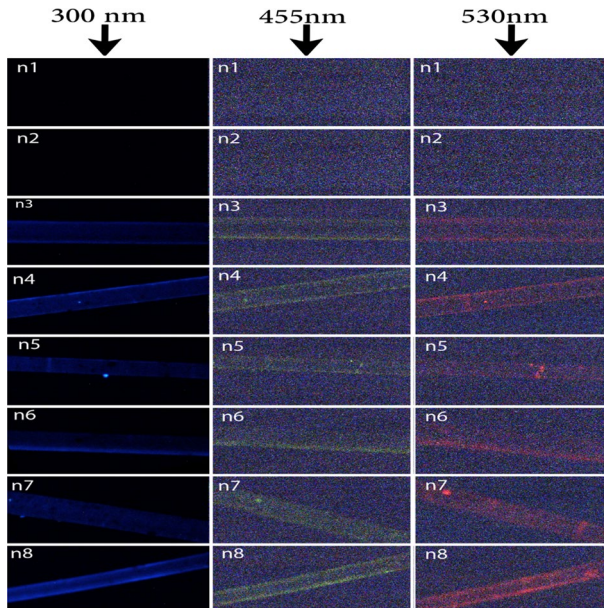
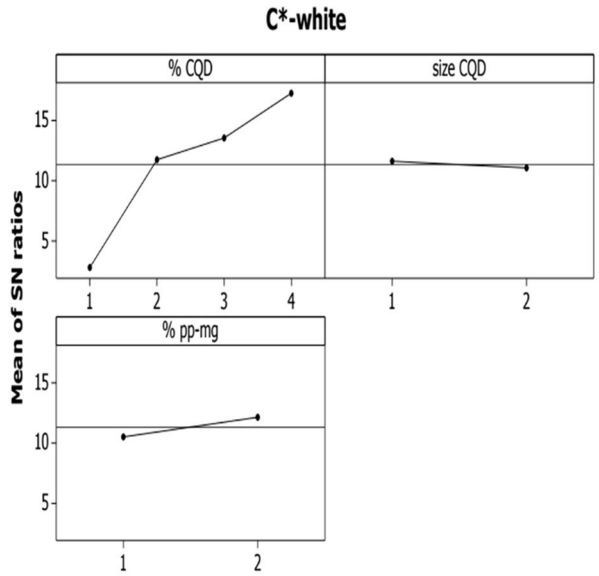


Fig. 15 Fluorescence microscopic images of PP/CQD nanocomposite excited at the wavelength of 300, 455, 530 nm

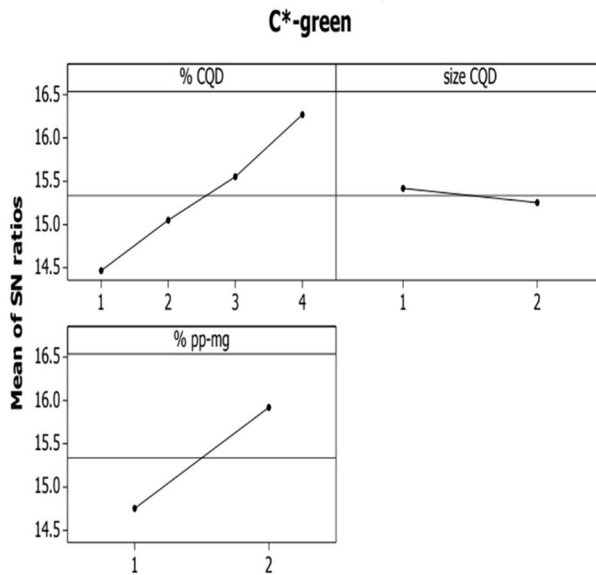
Figure 17 shows the Taguchi design analysis for the change of the lightness value (L^*) with CQD content, compatibilizer content, and CQD size. The lightness value was decreased with increasing CQD loading inside the polymer matrix, resulting in a darker shade, which is a direct consequence of light scattering due to the increase in the number of the nanoparticles. The samples containing the bigger-size nanoparticles showed lower lightness (L^*) because of increased light scattering.

The Taguchi design analysis for the chromaticity coordinate values (a^* and b^*) versus CQD loading on both green and white background standards is shown in Fig. 18. The results demonstrated a yellowish red hue with increasing CQD loading inside the polymer matrix [45]. The b^* value was shifted to positive; in other words, the hue was shifted to the yellow side, and the a^* value was shifted to the red side with increasing CQD loading inside the polymer matrix. The change of color was affected by the adsorbed state of CQD as light-emitting the nanoparticles. The color change of the samples was similar for the two background standards.

Besides, the redness and yellowness of the PP/CQD nanocomposite fibers were decreased with decreasing the size of the nanoparticles, and the samples' color shifted to blue and green (Fig. 19) [14].



Signal-to-noise: Larger is better

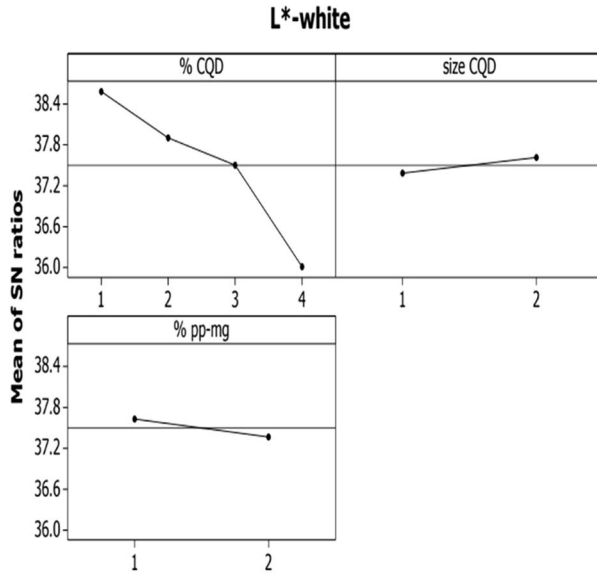


Signal-to-noise: Larger is better

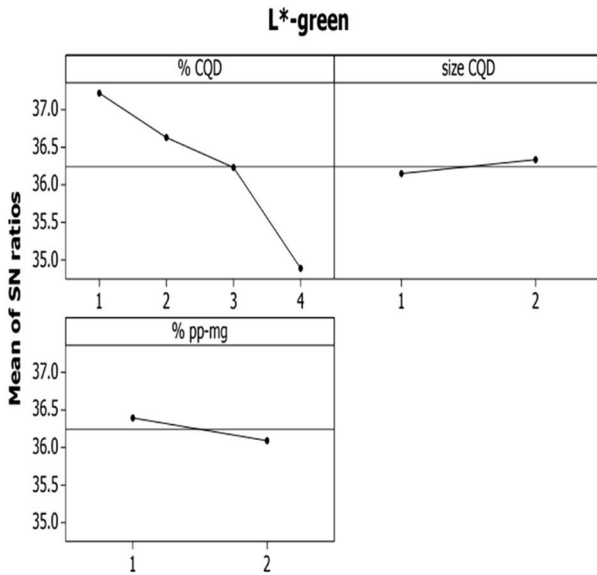
Fig. 16 Taguchi design analysis of the color purity in nanocomposite fibers on both white and green standards

Conclusion

In this study, PP/CQD nanocomposites containing different nanoparticle contents as



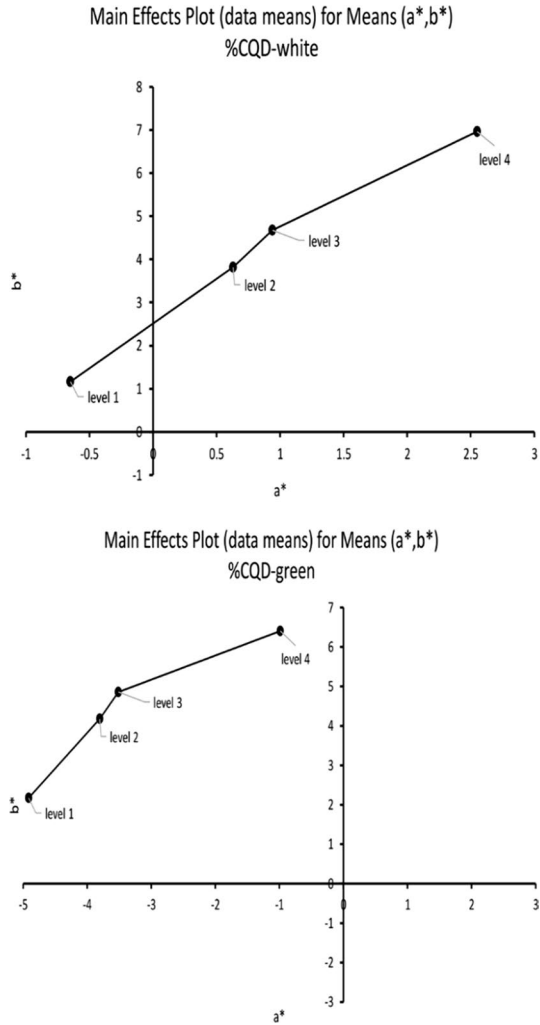
Signal-to-noise: Larger is better



Signal-to-noise: Larger is better

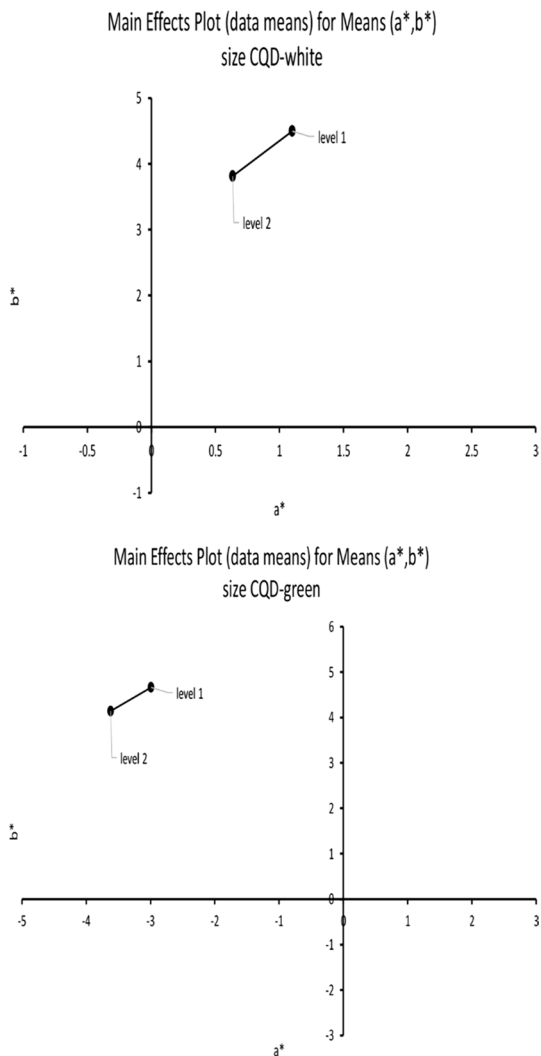
Fig. 17 Taguchi design analysis of the lightness value in nanocomposite fibers on both white and green standards

Fig. 18 Chromaticity diagrams of chroma coordinates (a^* , b^*) of the nanocomposite fibers on both white and green standards by Taguchi design analysis as a function of the concentration of the CQDs



well as different sizes of nanoparticles and different compatibilizer contents were prepared. The tensile strength measurement results showed that the sample with 1% wt. CQD, the CQD size of 2 nm, and 3% wt. compatibilizer exhibited the highest modulus and tensile strength. The degree of crystallinity of the nanocomposites decreased by increasing the nanoparticles' concentration in the polymer matrix. There was an increase in the degree of crystallinity of the samples containing the smaller-size nanoparticles. The addition of compatibilizer had a negative effect on the degree of crystallinity of the samples. The samples' helical content increased with the increase in CQD content the use of the smaller-size nanoparticles. The addition of the compatibilizer caused a decrease in the helical content of nanocomposite fibers. The PP/CQD nanocomposites fibers exhibited photoluminescence properties. The results confirmed that the optical properties of CQDs were preserved inside the

Fig. 19 Chromaticity diagrams of chroma coordinates (a^* , b^*) of the nanocomposite fibers on both white and green standards by Taguchi design analysis as a function of size of the CQDs



polymer matrix. The reflection spectrophotometry measurements showed that the purity value was increased with enhancing CQD loading inside the polymer matrix. The addition of the compatibilizer increased the purity value of nanocomposite fibers. The purity value was slightly reduced with the addition of the smaller-size nanoparticles. The lightness value was decreased with enhancing CQD loading and the bigger-size nanoparticles inside the polymer matrix. The results also demonstrated a yellowish red hue imparted to the nanocomposite fibers with improving CQD loading inside the polymer matrix. The amount of redness and yellowness of PP/CQD nanocomposite fibers was lower for the smaller-sized nanoparticles and trended to blue and green. In conclusion, the size, concentration, the addition of the compatibilizer, and dispersion of the carbon quantum dots within the polymer matrix exhibited

significant impacts on the specific optical behavior of PP/CQD nanocomposites fibers. The interaction between the carbon quantum dots and polymer was limited to the van der Waals weak force due to the lack of functional groups in the polypropylene polymer chains. Besides, PL was not quenched by a reabsorption mechanism, which was deduced from the overlapping between the nanocomposites' absorption and emission spectra. Therefore, PP/CQD nanocomposites fibers with photoluminescence properties can be potentially used in various applications such as smart clothing, sensors, photochemical reactions, and anti-counterfeiting technology.

References

1. Rossetti R, Brus L (1982) Electron–hole recombination emission as a probe of surface chemistry in aqueous cadmium sulfide colloids. *J Phys Chem* 86(23):4470–4472
2. Al-Ahmadi A (2012) Quantum dots—a variety of new applications. INTECH Open Access Publisher, Rijeka
3. Patil YS, Salunkhe PH, Navale YH, Patil VB, Ubale VP, Ghanwat AA (2020) Tetraphenylthiophene-thiazole-based π -conjugated polyazomethines: synthesis, characterization and gas sensing application. *Polym Bull* 77:2205–2226
4. Patil YS, Mahindrakar JN, Salunkhe PH, Ubale VP, Ghanwat AA (2019) Synthesis, characterization, and electrical and thermal stability of semiconducting π -conjugated polyazomethines containing a tetraphenylthiophene-oxazole unit. *J Electron Mater* 48:8067–8075
5. Patil YS, Salunkhe PH, Navale YH, Ubale VP, Patil VB, Maldar NN, Ghanwat AA (2018) Synthesis, characterization and conductivity study of co-polyazomethine polymer containing thiazole active ring. *AIP Conf Proc* 1989(1):020034
6. Paek K, Yang H, Lee J, Park J, Kim BJ (2014) Efficient colorimetric pH sensor based on responsive polymer–quantum dot integrated graphene oxide. *ACS Nano* 8(3):2848–2856
7. Li H, Kang Z, Liu Y, Lee S-T (2012) Carbon nanodots: synthesis, properties and applications. *J Mater Chem* 22(46):24230–24253
8. Luo PG, Sahu S, Yang S-T, Sonkar SK, Wang J, Wang H, LeCroy GE, Cao L, Sun Y-P (2013) Carbon “quantum” dots for optical bioimaging. *J Mater Chem B* 1(16):2116–2127
9. Zhang M, Yao Q, Lu C, Li Z, Wang W (2014) Layered double hydroxide-carbon dot composite: high-performance adsorbent for removal of anionic organic dye. *ACS Appl Mater Interfaces* 6(22):20225–20233
10. Alam A-M, Park B-Y, Ghouri ZK, Park M, Kim H-Y (2015) Synthesis of carbon quantum dots from cabbage with down- and up-conversion photoluminescence properties: excellent imaging agent for biomedical applications. *Green Chem* 17(7):3791–3797
11. Safaie B, Youssefi M, Rezaei B (2019) Rheological behavior of polypropylene/carbon quantum dot nanocomposites: the effects of particles size, particles/matrix interface adhesion, and particles loading. *Polym Bull*. <https://doi.org/10.1007/s00289-018-2611-8>
12. Xiao J, Cheng Y, Guo C, Liu X, Zhang B, Yuan S, Huang J (2019) Novel functional fiber loaded with carbon dots for the deep removal of Cr (VI) by adsorption and photocatalytic reduction. *J Environ Sci* 83:195–204
13. Zhao Z, Geng C, Zhao X, Xue Z, Quan F, Xia Y (2019) Preparation of CdTe/alginate textile fibres with controllable fluorescence emission through a wet-spinning process and application in the trace detection of Hg²⁺ ions. *Nanomaterials* 9(4):570
14. Huang Y, Liu J, Yu Y, Zuo S (2015) Preparation and multicolored fluorescent properties of CdTe quantum dots/polymethylmethacrylate composite films. *J Alloy Compd* 647:578–584
15. Wang Q, Wang H, Liu D, Du P, Liu P (2017) Synthesis of flake-shaped nitrogen-doped carbon quantum dot/polyaniline (N-CQD/PANI) nanocomposites via rapid-mixing polymerization and their application as electrode materials in supercapacitors. *Synth Met* 231:120–126

16. Yu L, Yue X, Yang R, Jing S, Qu L (2016) A sensitive and low toxicity electrochemical sensor for 2, 4-dichlorophenol based on the nanocomposite of carbon dots, hexadecyltrimethyl ammonium bromide and chitosan. *Sensors Actuators B: Chem* 224:241–247
17. Min S-Y, Bang J, Park J, Lee C-L, Lee S, Park J-J, Jeong U, Kim S, Lee T-W (2014) Electrospun polymer/quantum dot composite fibers as down conversion phosphor layers for white light-emitting diodes. *RSC Adv* 4(23):11585–11589
18. Saud PS, Pant B, Alam A-M, Ghouri ZK, Park M, Kim H-Y (2015) Carbon quantum dots anchored TiO₂ nanofibers: effective photocatalyst for waste water treatment. *Ceram Int* 41(9):11953–11959
19. Safaie B, Youssefi M, Rezaei B, Irannejad N (2018) Synthesis and properties of photoluminescent carbon quantum dot/polyacrylonitrile composite nanofibers. *Smart Sci* 6(2):117–124. <https://doi.org/10.1080/23080477.2017.1399318>
20. Safaie B, Youssefi M, Rezaei B (2018) Estimating the interphase properties of polypropylene/carbon quantum dot nanocomposite fibers by micromechanical modeling. *Colloid Polym Sci*. <https://doi.org/10.1007/s00396-018-4422-8>
21. Luongo J (1960) Infrared study of polypropylene. *J Appl Polym Sci* 3(9):302–309
22. Sclavons M, Franquinet P, Carlier V, Verfaillie G, Fallais I, Legras R et al (2000) Quantification of the maleic anhydride grafted onto polypropylene by chemical and viscosimetric titrations, and FTIR spectroscopy. *Polymer* 41(6):1989–1999
23. De Roover B, Sclavons M, Carlier V, Devaux J, Legras R, Momtaz A (1995) Molecular characterization of maleic anhydride-functionalized polypropylene. *J Polym Sci Part A: Polym Chem* 33(5):829–842
24. Bourlinos AB, Stassinopoulos A, Anglos D, Zboril R, Karakassides M, Giannelis EP (2008) Surface functionalized carbogenic quantum dots. *Small* 4(4):455–458
25. Law A, Simon L, Lee-Sullivan P (2008) Effects of thermal aging on isotactic polypropylene crystallinity. *Polym Eng Sci* 48(4):627–633
26. Youssefi M, Safaie B (2013) Effect of multi walled carbon nanotube on the crystalline structure of polypropylene fibers. *Fibers Polym* 14(10):1602–1607. <https://doi.org/10.1007/s12221-013-1602-5>
27. Weidinger A, Hermans P (1961) On the determination of the crystalline fraction of isotactic polypropylene from x-ray diffraction. *Macromol Chem Phys* 50(1):98–115
28. Jose MV, Dean D, Tyner J, Price G, Nyairo E (2007) Polypropylene/carbon nanotube nanocomposite fibers: process–morphology–property relationships. *J Appl Polym Sci* 103(6):3844–3850
29. Marco C, Naffakh M, Gómez MA, Santoro G, Ellis G (2011) The crystallization of polypropylene in multiwall carbon nanotube-based composites. *Polym Compos* 32(2):324–333
30. Fu S-Y, Feng X-Q, Lauke B, Mai Y-W (2008) Effects of particle size, particle/matrix interface adhesion and particle loading on mechanical properties of particulate–polymer composites. *Compos B Eng* 39(6):933–961. <https://doi.org/10.1016/j.compositesb.2008.01.002>
31. Zare Y, Rhee KY, Park SJ (2017) Modeling of tensile strength in polymer particulate nanocomposites based on material and interphase properties. *J Appl Polym Sci*. <https://doi.org/10.1002/app.44869>
32. Zhao H, Li RKY (2006) A study on the photo-degradation of zinc oxide (ZnO) filled polypropylene nanocomposites. *Polymer* 47(9):3207–3217. <https://doi.org/10.1016/j.polymer.2006.02.089>
33. Wu CL, Zhang MQ, Rong MZ, Friedrich K (2002) Tensile performance improvement of low nanoparticles filled-polypropylene composites. *Compos Sci Technol* 62(10):1327–1340
34. Wu CL, Zhang MQ, Rong MZ, Friedrich K (2005) Silica nanoparticles filled polypropylene: effects of particle surface treatment, matrix ductility and particle species on mechanical performance of the composites. *Compos Sci Technol* 65(3):635–645. <https://doi.org/10.1016/j.compscitech.2004.09.004>
35. Youssefi M, Safaie B (2018) The study on the mechanical properties of multi-walled carbon nanotube/polypropylene fibers. *J Inst Eng (India) Ser E* 99(1):37–42
36. Yang Y, Wen Z, Dong Y, Gao M (2006) Incorporating CdTe nanocrystals into polystyrene microspheres: towards robust fluorescent beads. *Small* 2(7):898–901
37. Li M, Zhang J, Zhang H, Liu Y, Wang C, Xu X, Tang Y, Yang B (2007) Electrospinning: a facile method to disperse fluorescent quantum dots in nanofibers without Förster resonance energy transfer. *Adv Func Mater* 17(17):3650–3656
38. Venugopal BR, Ravishankar N, Perrey CR, Shivakumara C, Rajamathi M (2006) Layered double hydroxide–CdSe quantum dot composites through colloidal processing: effect of host matrix–nanoparticle interaction on optical behavior. *J Phys Chem B* 110(2):772–776. <https://doi.org/10.1021/jp054774j>

39. Lee C, Pant B, Alam A-M, An T, Chung H-J, Hong S-T, Park S-J, Park M, Kim H-Y (2016) Bio-compatible and photoluminescent keratin/poly(vinyl alcohol)/carbon quantum dot nanofiber: A novel multipurpose electrospun mat. *Macromol Res*. <https://doi.org/10.1007/s13233-016-4124-3>
40. Liu Z, Chen Y, Ding W (2016) Preparation, dynamic rheological behavior, crystallization, and mechanical properties of inorganic whiskers reinforced polylactic acid/hydroxyapatite nanocomposites. *Journal of Applied Polymer Science*. <https://doi.org/10.1002/app.43381>
41. Van Puyvelde P, Velankar S, Moldenaers P (2001) Rheology and morphology of compatibilized polymer blends. *Curr Opin Colloid Interface Sci* 6(5–6):457–463
42. Sadeghi-Kiakhani M, Safapour S (2015) Improvement of the dyeing and fastness properties of a naphthalimide fluorescent dye using poly (amidoamine) dendrimer. *Color Technol* 131(2):142–148
43. Seto F, Muraoka Y, Sakamoto N, Kishida A, Akashi M (1999) Surface modification of synthetic fiber nonwoven fabrics with poly (acrylic acid) chains prepared by corona discharge induced grafting. *Die Angew Makromol Chem* 266(1):56–62
44. Pal A, Sk MP, Chattopadhyay A (2016) Conducting carbon dot-polypyrrole nanocomposite for sensitive detection of picric acid. *ACS Appl Mater Interfaces* 8(9):5758–5762. <https://doi.org/10.1021/acsami.5b11572>
45. Chen J, Meng C, Xie J, Pan L, Zhou D, Chen JN (2016) Laser eco-printing technology for silk fabric patterns. *Indian J Fibre Text Res (IJFTR)* 41(1):78–83

Publisher's Note Springer Nature remains neutral with regard to jurisdictional claims in published maps and institutional affiliations.